IET Renewable Power Generation

Research Article

IET Journals
The Institution of Engineering and Technology

ISSN 1752-1416
Received on 8th November 2019
Revised 14th February 2020
Accepted on 18th March 2020
doi: 10.1049/iet-rpg.2019.1307
www.ietdl.org

Supercapacitor-assisted LED (SCALED) technique for renewable energy systems: a very low frequency design approach with short-term DC-UPS capability eliminating battery banks

Dilini Jayananda[1] ✉, *Nihal Kularatna*[1], *David Alistair Steyn-Ross*[1]

[1]*School of Engineering, University of Waikato, Hamilton 3240, New Zealand*

✉ *E-mail: dukju1@students.waikato.ac.nz*

Abstract: The fluctuating nature of solar energy necessitates suitable energy storage systems. Compared to typical battery banks, supercapacitors offer longer cycle life eliminating the need to replace them regularly. However, compared to a typical maximum power point tracking controller, where the battery bank and resistive load fed by a switch-mode DC–DC converter allows impedance matching for maximum power transfer, a supercapacitor bank's significantly large capacitive load does not permit the typical impedance matching for maximum power transfer. This study compares the theoretical difference between battery versus supercapacitor energy storage, and highlights of the supercapacitor-assisted LED converter technique in achieving high-efficiency renewable energy-based DC-microgrid systems.

1 Introduction

With the proliferation of renewable energy sources, governments are encouraging end-users and product developers to reduce carbon footprint and dependency on fossil fuel to keep our planet's environment clean for future generations. In this regard designing products and systems with high end-to-end efficiency (ETEE) is a priority for both power electronic product designers and the research community. As depicted by Fig. 1, most electrical consumer products have electronic modules powered by a cascade of converters, typically starting with an AC–DC converter followed by multiple DC–DC converters. With ETEE essentially determined by the multiplication of efficiencies of the individual converter stages, ETEE drops geometrically with the number of converter stages. If the energy source is a 230 V AC, 50 Hz household power supply, the AC–DC converter followed by other DC–DC converters could have an ETEE as low as 73%, assuming each of the three converters has moderately high efficiencies of 90%. With renewable energy sources such as photovoltaic (PV) solar cells, providing DC outputs, we have the option of eliminating the first AC–DC converter achieving a significant rise in ETEE.

In 2014, the IEEE Committee on DC Energy Efficiency [1, 2] decided to promote DC-microgrid (DCMG)-based households as a novel approach for energy efficiency. Given the case of renewable sources such as PV solar cells providing a DC output with very short connections from the energy source to the load, Thomas Edison's concept of local DC power generation and distribution is quite practicable today. In order to conserve energy, both the distance between power generating sources and loads and the number of conversion stages should be minimised [2].

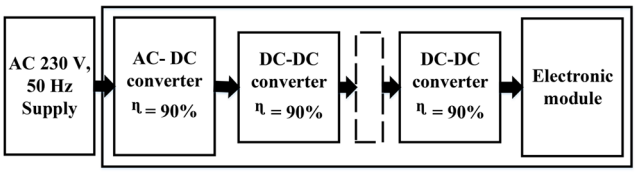

Fig. 1 *Energy flow within a typical electronic product or a system showing an ETEE of* $0.9^3 \cong 0.73$

As evidenced by the contributions to the three IEEE-ICDCM biennial conferences from 2015 to 2019 on the DCMG applications, the direct use of DC has been claimed as a key strategy for improving energy efficiency and reliability in buildings [3–6]. There are many components driving the growth of local DC electricity, few key points among these being [7]:

(i) Traditional AC centralised electrical power systems lose ~ 70% of the bulk generated electricity produced in transmission distribution and conversion [1].
(ii) Most consumer loads operate internally using DC power and the relative proportion of AC loads is decreasing over time.
(iii) DC power locally generated by renewable energy sources, such as solar panels and windmills, can reduce energy losses by as much as 30% compared with AC power systems.
(iv) DC based PV and wind power systems are more resilient than AC-based systems.

1.1 PV systems

Among the many types of sustainable energy sources, solar remains the most popular choice. This is due to the fact that solar PV energy is available at no running cost compared to conventional power generation systems. In addition, PV panels can be easily installed on the roof top or on the wall of commercial and residential buildings giving customer the choice of using either grid connected or off-grid PV systems.

Also, PV technology can be used to generate electricity for remote communities where the national grid is not accessible. Therefore, use of PV system is the most common local energy generation technique without any fossil fuel-based rotating machinery. US companies are increasingly turning to solar PV-based DCMG to offset energy costs. For example, in Minnesota, roof-top PV electricity cost 36 to 75% less than natural gas-based electricity during peak hours of the day [3].

Both grid connected and off-grid PV systems comprise a battery bank with a maximum power point tracking (MPPT) charge controller as depicted in Fig. 2. Use of a battery bank necessitates an MPPT charge controller, which typically consists of a switch-mode DC–DC converter to adjust the current and voltage to the battery bank to optimise charging while protecting the battery from

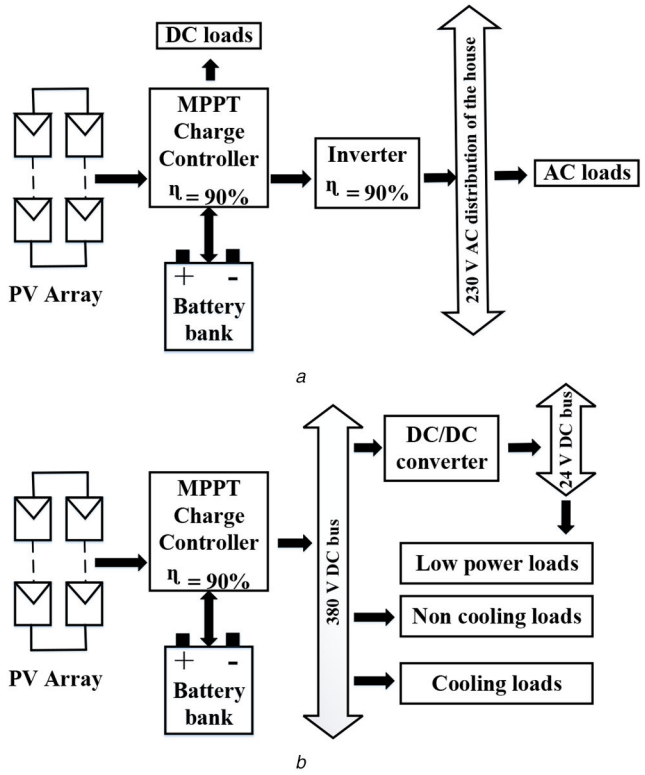

Fig. 2 *Existing PV system*
(a) Typical grid-connected PV system, ***(b)*** Typical off-grid PV system [8]

overcharging. In modern solar MPPT charge controllers, maximum efficiency is around 90% [9, 10]. When considering the grid-connected PV system depicted in Fig. 2*a*, each power conversion stage in this system wastes energy, thus leading to an unavoidable reduction of ETEE. A typical solar energy supply installed by commercial organisations based on an inverter is feeding the DC energy supply via the DC to AC converter on to the AC mains supply. This simple approach is disadvantaged by low conversion efficiency and low rebate rates for the energy fed to the grid via the inverter during daylight hours. Since we have two cascaded converters of 90% efficiency each, the overall ETEE of the system will be 81%. As the systems age, and their associated energy storage components deteriorate, ETEE can drop to much lower values. Accordingly, increasing the efficiency even by little as a few percent is economically worthwhile, and this motivates researchers to investigate new circuit topologies and techniques to boost efficiency levels. Fig. 2*b* depicts a typical off-grid DCMG system where the inverter has been eliminated to achieve improved ETEE ratings.

Fig. 3*a* depicts the typical characteristics of a solar panel showing its near constant current region (A–B), the narrow maximum power point (MPP) range of operation (B–C) and the typical voltage-source type operational region (C-D). It is vital to operate at the MPP in order to achieve the maximum efficiency for the overall system (includes PV array, converters, etc.). This MPP is located using MPP techniques such as perturb and observe (P&O), incremental conductance (IC), temperature method [9, 10]. Each of these tracking techniques has different efficiencies [9–15]. Theoretically, maximum possible load power occurs when the source resistance matches the load resistance [9]. This is achieved by changing the duty cycle of the switch-mode DC–DC converter in the MPPT charge controller.

1.2 Energy storage devices (ESDs) in PV systems

When DC loads are powered by a renewable energy source, ESD becomes essential for reliable operation due to the fluctuating nature of the energy source. The most common form of energy storage used in renewable energy based systems are rechargeable battery packs, typically lead-acid or lithium ion based chemistries. All rechargeable battery chemistries have limited calender life as

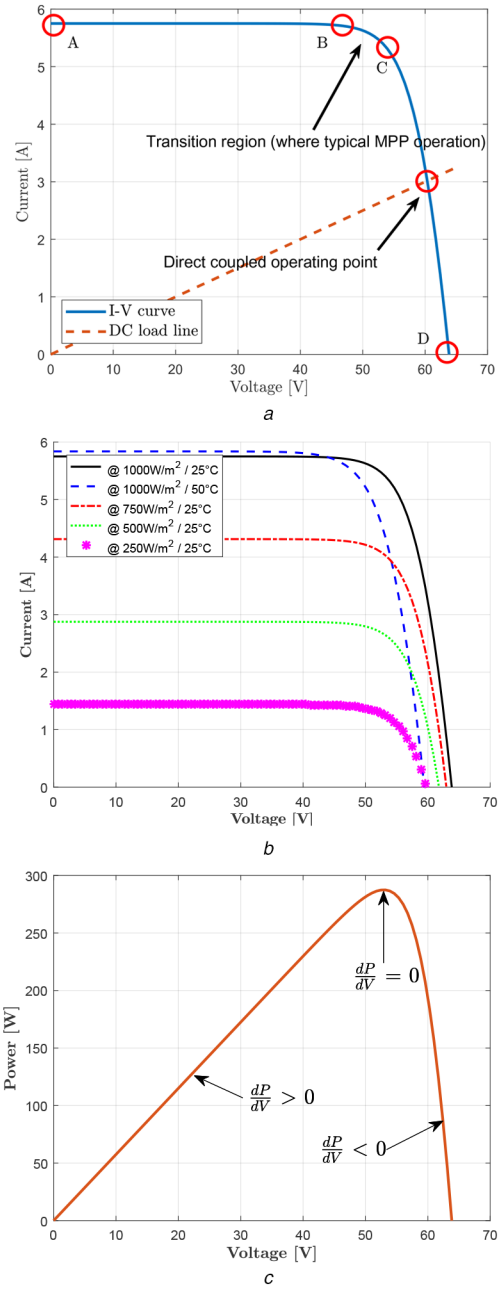

Fig. 3 *Characteristics curves of solar PV panel*
(a) PV current versus voltage characteristics with directly coupled operating point, ***(b)*** Current-voltage variations with irradiance, ***(c)*** Power versus voltage curve

well as charge–discharge life cycles, typically a few thousand though this count varies with the depth of discharge (DoD).

Supercapacitors (SCs) represent a newer ESD family for energy storage, that has excellent life-cycling but much lower energy density than electrochemical batteries. With the continuous developments of SC technology, material and manufacturing, it is now possible to adopt SCs as short-term ESDs in electronic systems with the advantage of low maintenance, extended life cycling and constant equivalent series resistance (ESR) with DoD. A comparison of the properties of SCs and batteries is shown in Table 1. Fig. 4*a* depicts the internal resistance variation with DoD of an electro-chemical battery versus a SC, based on a disposable 6 V lantern cell and a SC of value 3000 F.

1.2.1 Overview of SCs: Over the last decade SC technology has matured, with three different families of devices now being commercially available. Fig. 4 shows the position of the SCs as an ESD and the different types of SCs in terms of energy and power density. According to the Fig. 4, recent developments in SC technology has enabled battery-type hybrid SCs (CAPAbattery) to

Table 1 Comparison between electrochemical batteries and SCs [16]

Item	Supercaps	Batteries
charge time	1–60 s	1–5 h
discharge time	0.1–30 min	0.3–3 h
energy density, Wh/kg	1–20	20–100
power density, W/kg	10,000	50–200
cycle time	50,000–1,000,000	500–2000
charge/discharge efficiency	near 100%	70–85%
internal resistance	fractional mΩ	from 50 mΩ
or ESR	to several mΩ	to few Ω
	(constant with DoD)	(increases with DoD)

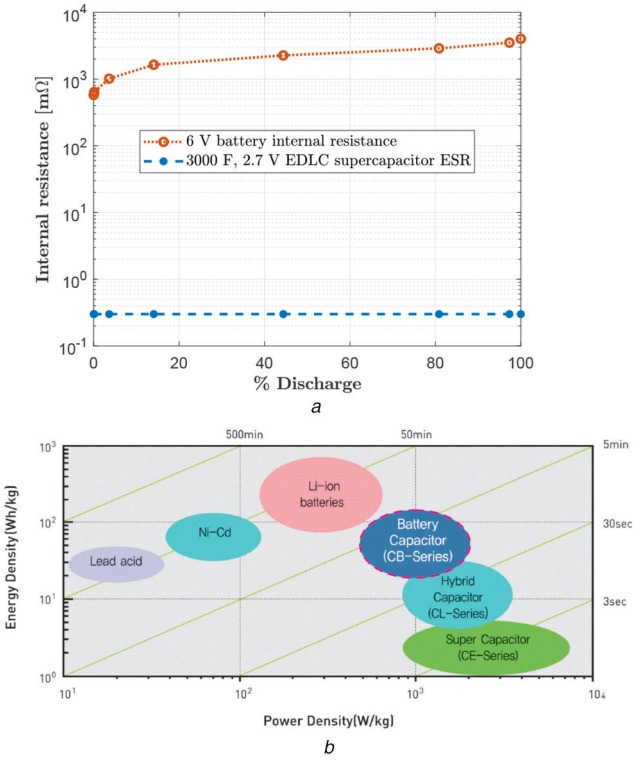

Fig. 4 *Comparison of SCs and batteries*
(a) Variation of internal resistance of a 3000 F, 2.7 V EDLC SC and an Energiser 6 V battery with percentage discharge, ***(b)*** Ragone plot of batteries and SCs [17]

Table 2 Comparison of commercially available SCs [17]

Parameter	EDLCs	Hybrid SCs	CAPAbatteries
energy density, Wh/L	5–8	10–14	50–120
power density, W/L	8000	2500–4000	1600–3200
cycle life, cycles	1,000,000	40,000–50,000	15,000–20,000
rated voltage, *V*	2.7	2.7	2.8
capacitance, *F*	1–3000	200–7500	1000–70,000

have fairly large power and energy density which allows designers to regard SC banks as a better alternative to lead acid batteries.

A parameter comparison of commercially available SC families is shown in Table 2. The newly introduced CAPAbattery type SCs have improved energy density, and capacitance. Despite the reduction of cycle life and power density compared to the more mature families of symmetrical EDLCs, they offer much higher cycle life and power density than commonly used lead-acid batteries. We have compared the performance characteristics of three different commercially available SC variations based on the following samples:

(i) 3000 F, 2.7 V electrostatic double layer SC (EDLC)

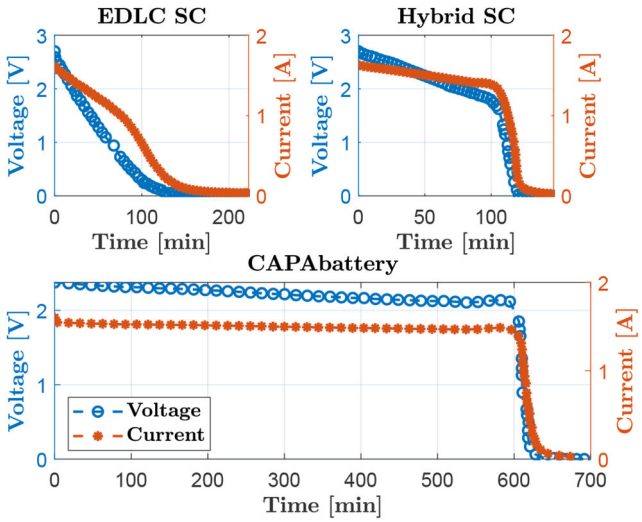

Fig. 5 *Discharge curves for three SC technologies for constant resistance (devices tested were 3000 F, 2.7 V EDLC SC, 7000 F, 2.7 V hybrid SC and 40,000 F, 2.8 V CAPAbattery respectively)*

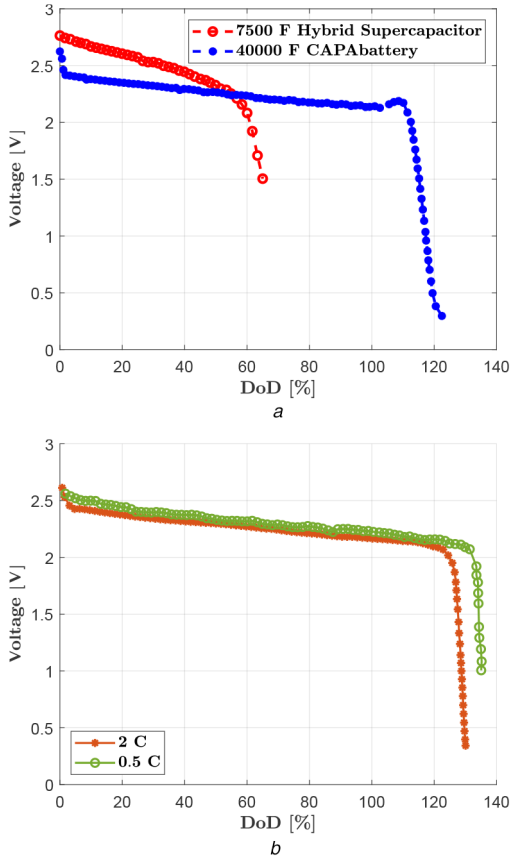

Fig. 6 *Constant current discharge curve for hybrid and CAPAbattery SCs*
(a) Discharge curve for hybrid and CAPAbattery SCs at *C*-rate, ***(b)*** Discharge curves for 40,000 F CAPAbattery at different *C*-rates

(ii) 7500 F, 2.7 V SC of the pseudo-capacitive hybrid technology (Hybrid SC)
(iii) 40,000 F, 2.8 V SC of the battery-type hybrid technology (CAPAbattery)

Tests were performed to compare the discharge voltage profiles for constant resistance discharge and constant current discharge.

(i) *Constant resistance discharge*
Fig. 5 depicts the behaviour of EDLC, hybrid and CAPAbattery SCs when discharged using constant resistance. We see that the discharge curve of an EDLC SC is similar to that of a normal

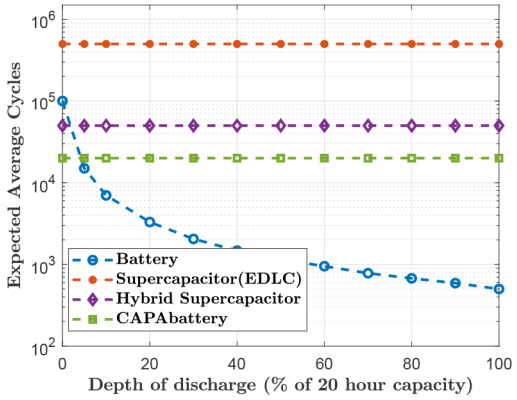

Fig. 7 *Variation of average life cycle for batteries and SCs with DoD [Data: SAMWHA capacitors]*

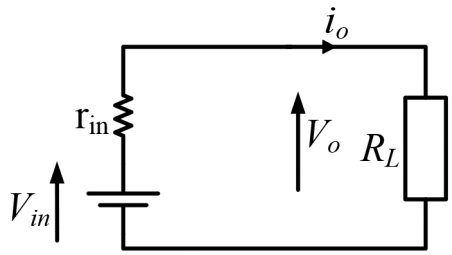

Fig. 8 *DC supply with external load connected*

electrolytic capacitor with voltage and current following a near-exponential decay. Discharge behaviour of SCs tend towards that of batteries as the technology moves from the EDLC to hybrid SC to CAPA battery. This highlights the trend towards improved energy density of SC technologies. From a voltage value of 2 V to the rated 2.7 V, the CAPAbattery can be approximated as a constant voltage source. The same applies to the hybrid SC from about 1.6 V to the rated 2.8 V.

Constant current discharge: the graphs in Fig. 5 shows that both hybrid SC and the CAPA battery discharge characteristics are closer to that of rechargeable batteries, with no evidence of an exponential or a near-exponential curve. From these graphs, we estimated that the 7500 F hybrid device could be considered as a 2.4 Ah battery and the 40,000 F CAPAbattery can be considered as a 12.2 Ah battery. Based on this authors have carried out a set of constant current discharges at C-rate for both samples. Results are given in Fig. 6*a* showing the respective voltage profiles at C-rate. As shown in Fig. 6*b*, the device shows similar behaviour as a battery with higher C-rates producing greater DoD than lower C-rates. Therefore just like in a battery CAPAbattery SC makes available more energy when discharged at lower currents.

It is well known that rechargeable batteries have reduced cycle life as DoD is increased. In contrast SCs have a cycle life that is independent of DoD. Fig. 7 shows the expected average cycles with DoD for batteries and SCs.

2 Maximising power delivery from a PV module to a battery

Recently developed PV technologies have demonstrated efficiencies of 20–28% [18], but most existing systems have conversion efficiencies of 9–20%. Another important property of PV arrays is the non-linear current voltage-characteristic as shown in Fig. 3*a*. Thus is essential to deliver maximum power from the PV panels to the connected load. Over the past three decades several useful methods have been proposed to extract maximum power from a solar panel array [9–15, 19].

As shown in Fig. 3*a*, a constant resistance DC load will create a stable operating point in the region beyond the knee area. Thus, for a direct-coupled system one must use an oversised PV array in order to ensure load's power requirements can be matched.

2.1 A review of MPPT concepts

Although there are several algorithms in common use for MPPT, they are all based on maximum power transfer theory. Let us consider the circuit shown in Fig. 8, where r_{in}, R_L is internal resistance of DC source and the external load respectively.

Based on Ohm's law, loop current $i_0 = V_{in}/(r_{in} + R_L)$, where V_{in} is the source voltage. The terminal voltage at the load, $V_0 = V_{in}R_L/(r_{in} + R_L)$. Thus the power delivered to the load can be derived as

$$P_L = \frac{V_{in}^2}{R_L}\left[\frac{1}{(1+\frac{r_{in}}{R_L})^2}\right] \tag{1}$$

Setting $dP_L/dR_L = 0$, we find that maximum power delivery to connected load is achieved when $r_{in} = R_L$.

Thus the impedance of the PV system must match that of the load in order to deliver maximum power. There are several commercially available MPPT techniques that are based on this impedance-matching theory. Table 3 provides a summary of MPPT techniques.

These six methods attempt to match the load impedance with the resistance of the solar panel. Major characteristics of these methods are summarised in Table 4.

2.2 Input impedance of switch mode DC–DC converter

A switch mode DC–DC converter, regardless of its topology, presents a negative incremental input impedance. Typical DC–DC converter in Fig. 9 works to maintain a constant output voltage V_o, at output power of P_0. For an ideal switch-mode DC–DC converter with 100% efficiency, following valuable relationships can be easily established [21].

The converter under continuous conduction mode (CCM) acts as a DC transformer with a turns ratio of n which leads to the useful relationship of,

$$r_{in} = n^2 R_L \tag{2}$$

where R_L is the load resistance ($R_L = V_0/i_0$).

In accordance with (2) and Table 5 it can be observed that the input impedance of a switched mode DC–DC converter is a function of the duty cycle of the converter. Hence by varying D it is possible to vary the effective input impedance of the converter. This approach is used in MPPT controllers to match the PV array resistance with the load resistance. Fig. 10 depicts the variation of input resistance with duty cycle ratio for the above converter types.

Let's analyse a situation where a resistive load buffered by a battery pack is connected to the output of a buck converter. By considering Fig. 11, the Thevenin resistance of the combined battery and load is

$$R_0 = \frac{R_L r_b}{R_L + r_b} \tag{3}$$

with r_b being the internal resistance of the battery. Therefore r_{in} can be modified as

$$r_{in} = \frac{R_0}{D^2} \tag{4}$$

showing that, r_{in} varies from $\infty \rightarrow R_0$ as D goes from 0 to 1. With the variation of irradiance and temperature, the MPP of PV panel also changes. Hence, by varying the duty cycle it is possible to match the load impedance with PV module impedance to extract maximum power.

Table 3 Summary of MPPT algorithms

Method	Description
fixed duty	' Off-line' method, no feedback. Load impedance is adjusted to match with PV module resistance once at set-up time. Variation of MPP due to temperature and irradiance changes are disregarded [11].
Constant voltage	It is assumed $V_{MPP} = kV_{OC}$ where V_{MPP} is MPP voltage, $0.7 \leq k \leq 0.8$ and V_{OC} is the open circuit voltage of the PV module under standard test conditions (1000 Wm^{-2}, 25^0C). Cannot capture the complexities of shading. Good for regions where temperature variation is low.
P&O	From Fig. 3*c* it is clear that power produced by the PV module increases with the panel voltage before MPP and decreases after reaching MPP. P&O algorithm compares the power at the previous time step ($P[k-1]$) with that for next step ($P[k]$), so it can increase or decrease the reference voltage (V_{ref}) of the switched mode DC–DC converter in order to align the operating point towards MPP optimum.Independent from PV panel/manufacturer. Not responding quickly to fast changes in environmental conditions.
IC	Proposed to overcome some limitations of the P&O method. Based on the fact that slope of the $P--V$ characteristics curve is zero at MPP $\left(\frac{dp}{dv} = 0\right)$, positive in the left, and negative in the right as shown in Fig. 3*c*. MPP is related to the incremental change in conductance of the PV array. By manipulating following two equations peak power delivery point can be located. $\frac{dp}{dv} = \frac{d(vi)}{dv} = i + v\frac{di}{dv} = 0;\ \frac{di}{dv} = -\frac{i}{v}$ The algorithm increases or decreases the voltage across the PV array by changing the V_{ref} reference voltage presented to the switched mode DC–DC converter. Fast response to abstain transients in environmental conditions.
beta method	The beta method approximates the MPP using an intermediate variable β [20] that is a function of panel voltage V_{PV} and current I_{PV} as: $\beta(V_{PV}, I_{PV}) = \ln\left(\frac{I_{PV}}{V_{PV}}\right) - cV_{PV}$ and which simplifies to a constant at the optimum operating point. Ideally the electrical parameters of the PV module should be known in order to estimate the optimal performance point which can reduce the effectiveness of this method.
temperature method	Uses low cost temperature sensors to tune the MPP algorithm function, because the MPP changes with temperature[20]. Non-uniform temperature distributions across the PV array can make implementation problematic. The voltage tuning equation is; $V_{MPP}(T) = V_{MPP}(T_{ref}) + K_{TVoc}(T - T_{ref})$ where V_{MPP} is MPP voltage, *T* is the panel temperature, K_{TVoc} is the temperature coefficient of V_{MPP}, and T_{ref} is reference temperature. Sensors may be poorly calibrated or not correctly attached, providing wrong measurements of PV temperature.

Table 4 Major characteristics of MPPT algorithms[20]

Method	Dependency of PV array	Tracking factor (TF)	Implementation complexity	Accuracy	Sensors
fixed duty	no	0.87	very simple	very low	none
constant voltage	yes	0.92	simple	low	*V*
P&O	no	0.96	simple	very high	*V*, *I*
IC	no	0.96	medium	very high	*V*, *I*
beta	yes	0.99	medium	very high	*V*, *I*
temperature	yes	0.98	simple	very high	*V*, Temp

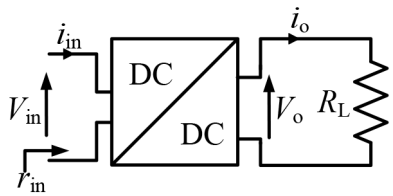

Fig. 9 *Block diagram of loaded switched mode DC–DC converter*

Table 5 Transformation coefficient *n* for switched mode converter (*D* is the duty ration of the converter)

Converter type	Transformation coefficient (*n*)
buck converter	$1/D$
boost converter	$1 - D$
buck–boost converter	$(1 - D)/D$

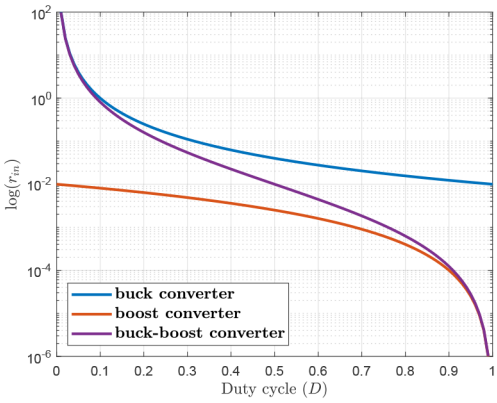

Fig. 10 *Variation of input resistance r_{in} of an ideal switching converter under CCM with duty cycle D*

3 Feasibility of replacing a battery pack with SCs

With recent advances such as hybrid SCs and CAPAbatteries offering higher energy densities, battery packs may be easily replaced by the higher life cycle based SC banks, with the secondary advantage of the constant ESR irrespective of the DoD. Nevertheless, if a battery bank is replaced solely by an SC bank, existing MPPT schemes are not adaptable since the load becomes predominantly capacitive, compared to the case of a battery bank and resistive load which allows simple impedance matching based on the effective resistive load seen by the solar panel. Following

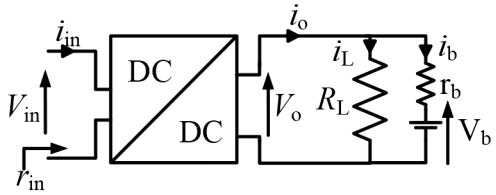

Fig. 11 *Buck converter with resistive load is buffered by a battery bank*

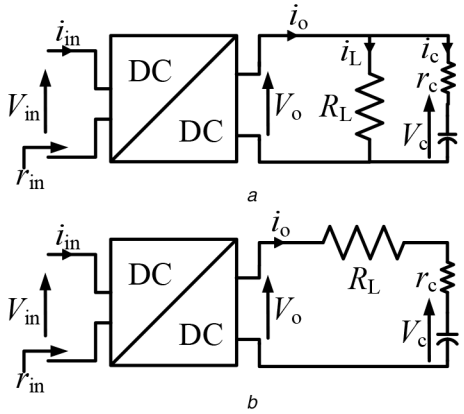

Fig. 12 *Buck converter with a capacitor at the output*
(a) Parallel connection, ***(b)*** Series connection

sections provide a summary of the two cases, namely parallel and series connection of the capacitor.

3.1 Capacitor connected to the output of a buck converter

Parallel connection of the capacitor: consider Fig. 12*a* where load is buffered with a SC bank.

Using Ohm's law output current i_0 can be derived as

$$i_0 = i_c + i_L = \frac{V_0}{R_L r_c}\left(r_c + R_L e^{\frac{-t}{r_c C}}\right) \tag{5}$$

where C is the capacitance and r_c is ESR of the capacitor. Capacitor is assumed to start with zero initial voltage.

Using (5), the general expression for Thevenin resistance R_0 can be obtained as

$$R_0 = \frac{R_L r_c}{r_c + R_L e^{\frac{-t}{r_c C}}} \tag{6}$$

Accordingly, r_{in} of the buck converter will be

$$r_{in} = \frac{R_L r_c}{D^2\left(r_c + R_L e^{\frac{-t}{r_c C}}\right)} \tag{7}$$

From (7) it can be seen that, when $t = 0$ (initially) r_{in} of the DC–DC converter is $R_L r_c/(D^2(R_L + r_c))$, and as $t \to \infty$ input impedance r_{in} approaches $D^2 R_L$.

Series connection of the capacitor: considering Fig. 12*b*, i_0 can be derived as

$$i_0 = \frac{V_0}{R_L + r_c}\exp(-t/(r_c + R_L)C) \tag{8}$$

So we estimate the input resistance of the DC–DC converter r_{in} to be

$$r_{in} = \frac{V_0}{D^2 i_0} = \frac{(R_L + r_c)\exp(t/(r_c + R_L)C)}{D^2} \tag{9}$$

When considering (9), it is clear that in the case of series connection, input impedance r_{in} varies from $(R_L + r_c)$ to ∞ as t goes from $0 \to \infty$.

Fig. 13 depicts the behaviour of input impedance of the buck converter when SC bank is used as the sole ESD for both parallel and series connection.

Compared to the case of a battery bank resulting in an input resistance given by (4), a SC bank makes the input resistance of the converter dependent on the state of the charge of the SC bank, which is also related to the time constant of the output circuit. This makes it extremely difficult to adapt the existing MPPT schemes into SC-based ESD systems. This is clear from the (7) to (9). More details on this are available in [8].

4 Loss circumvention concept (LCC) applied to RC loop fed by a DC voltage source

With reference to Fig. 14, two cases of capacitor charging are compared. In Fig. 14*a*, the capacitor is directly charged from constant DC voltage source of V_s starting from 0 V. In this case the energy stored in the capacitor in terms of maximum charge accumulated by the capacitor (Q) and the DC source voltage is given by

$$E_C = \frac{CV_s^2}{2} = \frac{QV_s}{2} \tag{10}$$

Also, we can prove that the total loss in the capacitor charging loop is also equal to $CV_s^2/2$ irrespective of the total loop resistance given by $r_p + r_c + r_s$. Therefore, efficiency of capacitor charging loop is only 50%.

Fig. 14*b* indicates a special case where a useful resistive load R_L (such as a heater) is inserted into the same charging loop where $r_{lp} = r_p + r_c + r_s$. Under this situation with the resistive load consuming energy in useful manner, the efficiency of capacitor charging circuit in Fig. 14*b* is given,

$$\eta = \frac{E_C + E_{R_L}}{E_C + E_{R_L} + E_{r_{lp}}} > 50\% \tag{11}$$

Total loss incurred in charging the capacitor from 0 to V_s is

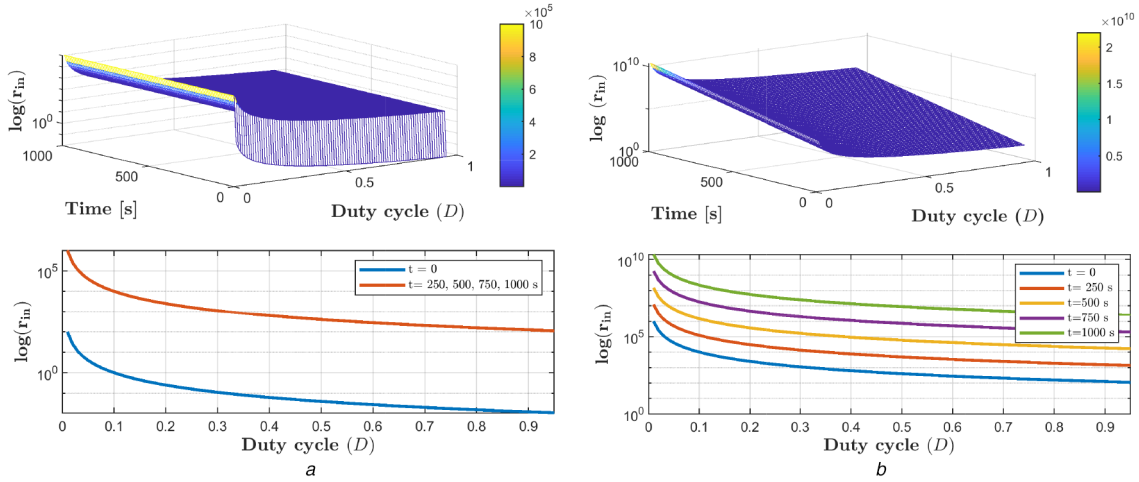

Fig. 13 *Variation of r_{in} for buck converter with capacitor at output ($C = 1\,F$, $R_L = 100\,\Omega$, $r_c = 0.01\,\Omega$)*
(a) Parallel connection of capacitor, ***(b)*** Series connection of capacitor

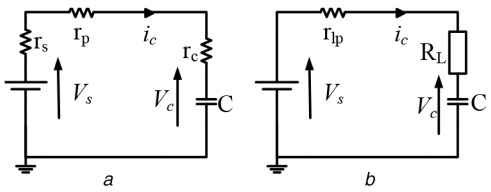

Fig. 14 *RC charging loop*
(a) Basic *RC* charging loop, ***(b)*** Modified *RC* charging loop with LCC

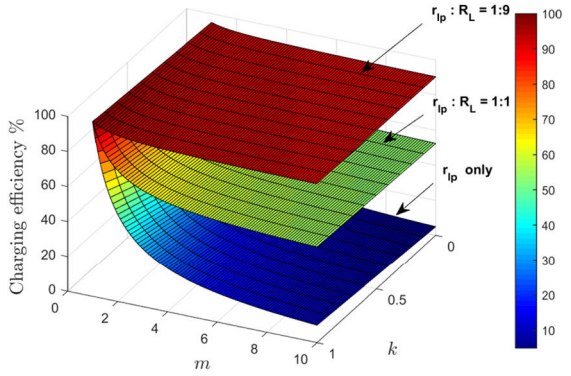

Fig. 15 *Graphical representation of the circuit behaviour in terms of efficiency versus m (over-voltage factor) and k (pre-charge factor)*

$$E_{r_{lp}} = \left(\frac{r_{lp}}{r_{lp} + R_L}\right) E_{Loss} \tag{12}$$

Thus by inserting a useful resistive load (e.g. heater, lamp load, LDO, loaded inverter), the capacitor charging circuit can be made more energy efficient.

Combining the above LCC with the case of a SC bank extending the time constant by several orders of magnitude, several SC-assisted (SCA) techniques have been developed at the University of Waikato [22]. Some examples are low drop-out regulator (SCALDO), temperature modification apparatus, high density inverter, surge absorber and LED lighting converter (supercapacitor-assisted LED (SCALED)) [8, 23–25].

In these SCA techniques, the above simplified theory is generally extended by operating the circuit with a higher DC source voltage based on multiplication factor m (> 1) with a SC of rated voltage V_w ($< V_s$) and initial voltage of kV_w ($k < 1$). For this case charging process related to Figs. 15 and 16 has an efficiency is given by $\eta = (1 + k)/2m$ [26].

Since SCs have very low ESR and very large capacitance, if a SC is charged or discharged with a constant current of I_{SC}, voltage change ΔV_{SC} across the SC after a time period of Δt is given by $C\Delta V_{SC} = I_{SC}\Delta t$. This indicates that a series connected SC can be

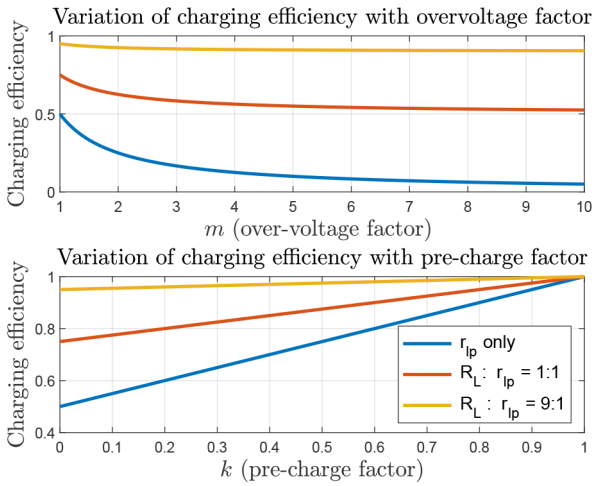

Fig. 16 *Variation of charging efficiency*

treated as a lossless voltage dropper. The SCA designs for DC conversion (SCALDO) and LED lighting (SCALED) are based on this LCC.

4.1 SC-assisted low drop-out regulator

The first application of this LCC was the 2011 patented SCALDO technique [27], depicted in Fig. 17. The series capacitor will pass current as it charges and discharges cyclically, storing and releasing energy. Fig. 17*a* depicts the charging phase where the SC is charged from the unregulated DC voltage source until input voltage of LDO (V_{in}) reaches the minimum allowable voltage for regulation. Then the SC is connected parallel with input of the LDO while disconnecting from the unregulated DC source as shown in Fig. 17*b*, to release the stored energy in the SC. This results in a linear regulator based on an LDO whose ETEE can be improved by a factor of, (see equation below) For the two cases of $5 - 3.33$ V and $12 - 5$ V, this factor is 1.33 and 2, respectively. The SCALDO converter, which is not a variation of switched capacitor converters [16, 28], has other useful characteristics such as:

(i) DC UPS capability (by over-sizing the SC)
(ii) Low noise and high slew rate output capability
(iii) Extra low-frequency operation eliminating RFI/EMI issues typical of high frequency switching DC–DC converters

More details of the SCALDO converter are available in [1, 16, 23, 28, 29].

In this case, the loaded LDO acts as the useful resistive load (R_L) with a SC taking the role of the capacitor C in Fig. 14.

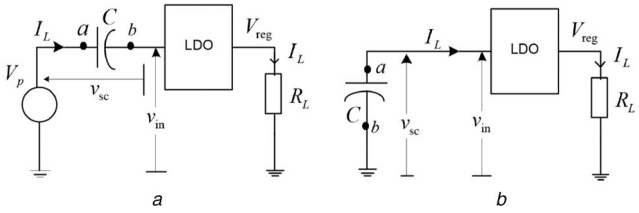

Fig. 17 *SCALDO converter*
(a) SC bank charging while minimizing series dissipation, ***(b)*** Releasing stored energy in SC bank [26]

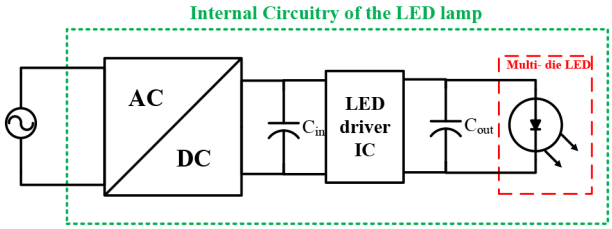

Fig. 18 *Internal circuitry of a commercially available LED lamp*

Table 6 Comparison between LED lamps and conventional lamps [8]

Parameter	Incandescent	CFL	LED
avg. life span, h	1200	8000	50000
wattage, W	60	13–15	6–8
annual operating cost, USD	330	80	30
Lumen per watt	10–20	50–70	112
CO_2 emission, kg/y	2000	500	200
electricity usage per year, kWh/yr (30 incandescent lamps per year equivalent)	3300	800	300

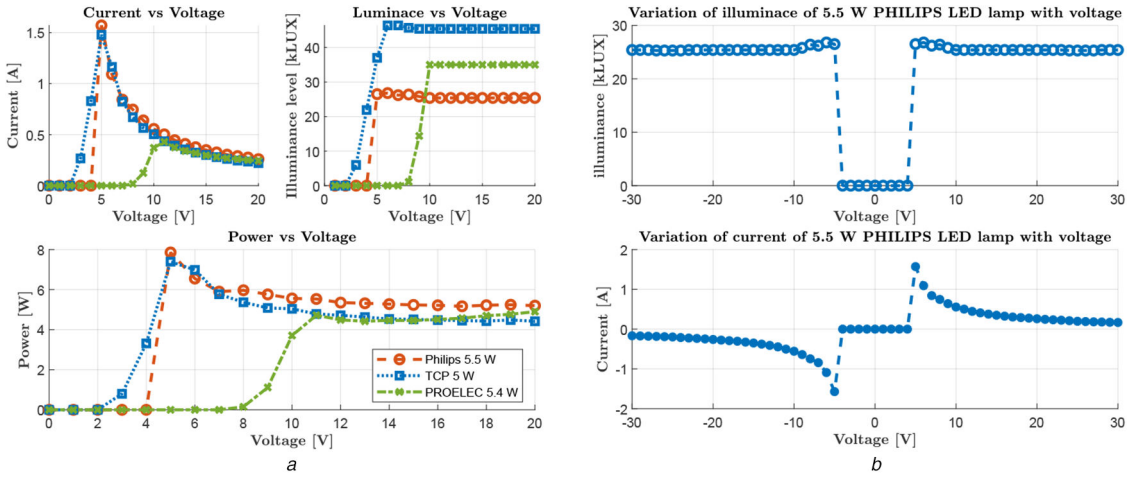

Fig. 19 *Practical behaviour of commercially available LED lamps*
(a) Characteristics curves of commercially available LED lamps, ***(b)*** DC voltage reversal capability of Philips 5.5 W LED lamps

Section 5 describes some characteristics of low-voltage LED luminaries, and Section 6 extends the SCALED technique to DCMGs.

5 Operational details of low voltage (12 V) LED lamps

LED lamps have much higher luminous efficacy compared to compact fluorescent lamps and incandescent lamps, and they play a major role in efficient illumination of modern buildings. Typically, LED lamps combine solid state lighting with power electronic converters as shown in Fig. 18. According to the data available for 2012, USA saved about $700 million of annual energy cost by installing LED lamps [30]. A detailed comparison between LED lamps and conventional lamps (CFL and incandescent) is given in Table 6.

5.1 Practical performance of 12 V LED lamps

A set of laboratory experiments were carried to characterise the operational behaviour of 12 V LED lamps. Variation of luminance, current drawn, and power consumption with the voltage across the lamp were recorded for three brands of commercially available LED lamps.

Fig. 19*a* shows the operational behaviour of the tested LED lamps. As depicted in Fig. 19*a*, we see that power consumption and brightness of the LED lamps remains constant for a wide range of DC voltages (9–20 V) around the nominal value of 12 V. Two

$$\text{efficiency improvement factor} = \frac{\text{ETEE of SCALDO regulator}}{\text{ETEE of related linear regulator}}$$

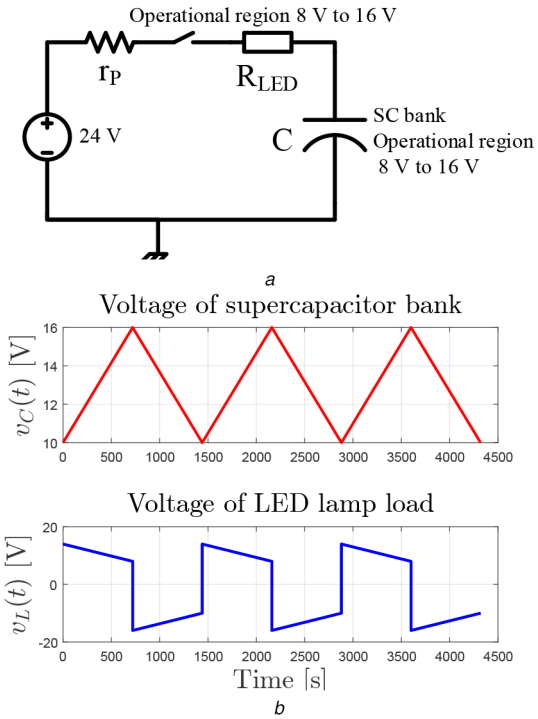

Fig. 20 *Concept of proposed SCALED converter*
(a) Modified RC charging loop with LED lamp, ***(b)*** Voltage waveforms for SC bank and LED lamp load [31]

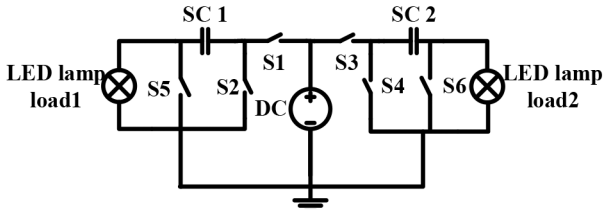

Fig. 21 *The proposed SCALED converter*

Table 7 Switching arrangement of SCALED converter

Mode	S1	S2	S3	S4	S5	S6
initial charging	on	off	on	off	on	on
SC2 charging and SC1 discharging	off	on	on	off	off	off
SC2 discharging and SC1 charging	on	off	off	on	off	off

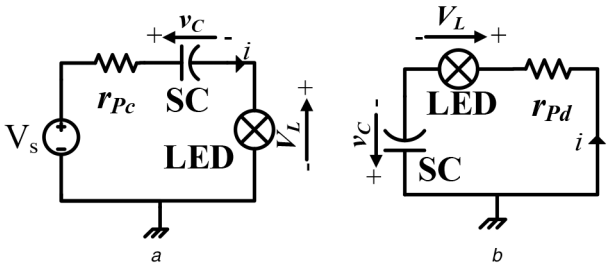

Fig. 22 *Basic configurations of SCALED converter*
(a) SC charging phase, ***(b)*** SC discharging phase

lamps draw the highest current around 5 V. This maximum current depends on the wattage rating of the lamp as well as the driver circuit. Fig. 19*b* shows this characteristic for Philips 5.5 W LED lamp. These results are based on our own laboratory measurements, since these data are not provided by the lamp manufacturers.

In summary, commercially available 12 V LED lamps have of the following desirable features:

(i) Ability to operate with positive or negative DC voltages.
(ii) Ability to operate over a wide range of AC/DC voltages without compromising brightness.
(iii) Ability to operate as constant power load in the constant brightness region.

These three features were utilised in developing the SCALED technique useful in the DCMG environments. Fig. 19*b* depicts the voltage reversal capability of the Phillips 5.5 W LED lamps, which was also utilised to reduce the switch counts while developing the SCALED converter.

6 SCALED technique

The SCALED converter uses the same loss circumvention principle discussed in Section 4. Here, 12 V DC operable LED lamps serve as the ‘ useful load’ in the *RC* circuit shown in Fig. 14*b*, consuming energy while charging the capacitor. If the DC equivalent resistance of LED lamps (R_{LED}) is much higher than the parasitic resistance of the loop (r_P) in Fig. 20*a*, most of the energy wasted in the *RC* charging loop is utilised by the LED lamps. Fig. 20 depicts a case of nominal 24 V DC voltage source, switch and the LED lamp working in series, charging an SC bank which is operating with a DC voltage range of 8–16 V. Fig. 20*b* shows the voltage across SC bank and LED lamp assuming that $R_{LED} \gg r_P$. The switch should be operated in such a way that both LED lamp and SC bank are not exposed to any voltage higher than the maximum limit of the operational voltage region. When the SC bank reaches the upper limit, the excess energy within the bank should be released to the load. By using an adequately rated SC bank (approximately twice or larger DC voltage capability of LED bank) with LED lamp, SCALED technique helps to significantly reduce the losses in the RC loop. Theoretical details of the technique are available in [8, 31–33].

6.1 Actual SCALED design example

Two important properties of 12 V LED lamps: (i) ability to operate with positive or negative DC voltages, (ii) ability to operate over a wide range of AC/DC voltages without compromising brightness, were used during the design phase of the SCALED converter. In order to use SC banks as practical ESDs within an overall system with charge balance over each cycle, the concept shown in Fig. 21 was developed. This converter incorporates three different modes of operation as depicted in Table 7.

At the start-up phase (initial phase) of the converter, SC banks 1 and 2 will charge up to 20 V and 9 V respectively by directly connecting PV module to SC banks and disconnecting the two LED lamp banks. Once both SC banks are charged up to required voltage levels, the converter commences normal operation in which one SC bank charges to 20 V through LED lamps while the other SC bank discharges to the other LED lamps.

When first SC bank is charged to 20 V, it will switch to discharging phase while the other bank now switches to charging phase and cycle repeats. Due to the ability of LED lamps to operate within wide range of positive or negative voltages around the nominal value without degradation of brightness, this technique can cope with large fluctuations of solar irradiance. In addition, SC banks are able to provide power to LED lamp loads during low irradiance levels to provide short-term (in order of minutes) DC-UPS capability. In this converter switches S2 and S4 help to preserve the charge balance of respective SC banks by alternately switching S1 and S3 as a pair. In order to maintain the switching sequence shown in Table 7, using a controller is compulsory. This method is applicable for large LED lighting loads such as 24 V, 48 V or over 100 V cases. Fluctuations in solar irradiance can be effectively accommodated by appropriate sizing of the SC banks. More details on implementation of this new technique is available in [8, 31–33].

This converter has two main configurations as shown in Fig. 22, and is based on fact that LED lamps are capable of operating with both positive and negative rails. Analysis of charging phase and discharging phase of SCALED converter is given below in a summary form. Details are presented in [31, 33].

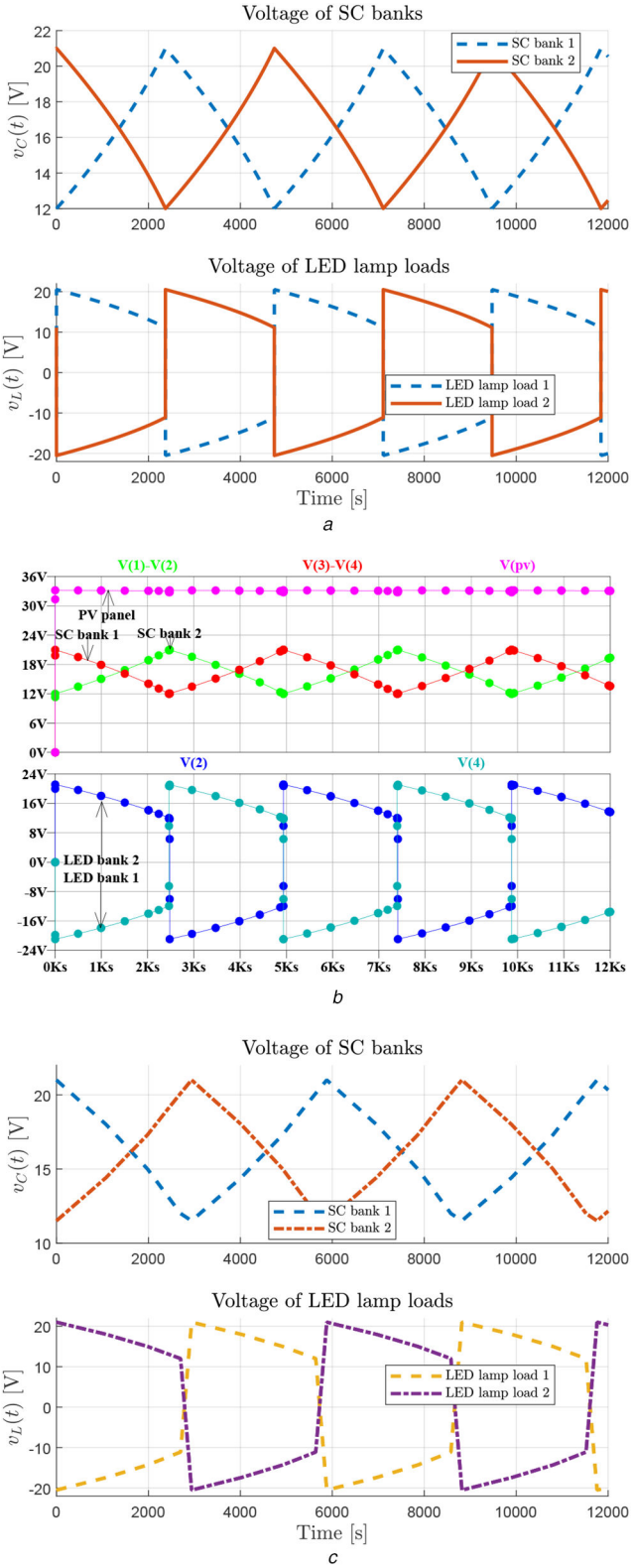

Fig. 23 *Simulation and laboratory test results of SCALED converter*
(a) MATLAB simulation results, ***(b)*** Spice simulation results, ***(c)*** Laboratory test results

The SCALED converter was modelled using MATLAB and Spice simulations, and compared with experimental data gathered from the pilot site at the jetty areas of the Ports of Auckland.

SCALED charging phase: considering Fig. 22*a*, voltage across the LED lamp is:

$$V_L = V_S - v_C - ir_{Pc} \tag{13}$$

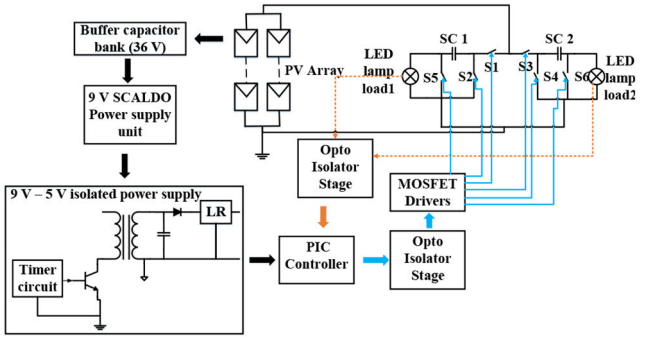

Fig. 24 *Simplified block diagram of implemented SCALED converter*

where i is the instantaneous loop current and r_{Pc} is the loop resistance. Since the power consumption P_0 of the LED lamp is constant over the constant brightness region (see Section 5) and $i = C\mathrm{d}v_C/\mathrm{d}t$, (13) can be modified as:

$$\left(V_S - v_C - r_{Pc} \cdot C\frac{\mathrm{d}v_C}{\mathrm{d}t}\right)\frac{\mathrm{d}v_C}{\mathrm{d}t} = \frac{P_0}{C} \tag{14}$$

Solving (14) for $\mathrm{d}v_C/\mathrm{d}t$, it is possible to derive a differential equation that can be evaluated using numerical integration,

$$\frac{\mathrm{d}v_C}{\mathrm{d}t} = \frac{(V_S - v_C) - \sqrt{(V_S - v_C)^2 - 4r_{Pc}P_0}}{2r_{Pc}C} \tag{15}$$

where C is the capacitance.

SCALED discharging phase: applying Ohm's law to Fig. 22*b*, the expression for capacitor voltage v_C can be derived in terms of capacitance C, loop resistance r_{Pd} and power of the LED lamp P_0,

$$\left(v_C + r_{Pd} \cdot C\frac{\mathrm{d}v_C}{\mathrm{d}t}\right)\frac{\mathrm{d}v_C}{\mathrm{d}t} = -\frac{P_0}{C} \tag{16}$$

which can be rewritten as

$$\frac{\mathrm{d}v_C}{\mathrm{d}t} = \frac{-v_C + \sqrt{v_C^2 - 4r_{Pd}P_0}}{2r_{Pd}C} \tag{17}$$

Since (15) and (17) are non-linear differential equations, Euler numerical integration was carried out using MATLAB to find the solutions. The switching sequences in Table 7 were used in MATLAB code to simulate the full SCALED converter. The authors also used the LTspice simulation package to verify the MATLAB and experimental results. For the Spice simulation a model for the PV panel was created using its characteristic equations. Simulation and laboratory test results of SCALED converter are presented in Fig. 23. Simulation and analytical details of SCALED converter are available in [31, 33].

6.2 Application in Ports of Auckland Ltd. (POAL) DCMG container

The SCALED converter was developed with a pilot grant from POAL. An experimental shipping container used as an office cubicle in the jetty area was illuminated by commercially available 12 V LED lamps. Fig. 24 depicts the simplified block diagram of the overall system installed in POAL DCMG container. A summary of components used for implementation is given in Table 8.

Testing of the full version of the POAL SCALED system was carried by using a CSUN250-60P PV panel as the energy source. The open circuit of the PV panel was 37.3 V, SC banks were charged to 20 V and discharged to 12 V to avoid the unnecessary higher voltage across LED lamp loads during the charging phase of SC banks. A GL240 data logger was used to acquire the experimental data at the POAL site. Operational behaviour of SCALED converter for three different days with average irradiance

Table 8 Summary of components used for SCALED converter

Component	Specification
SCs	Two 166 F, 51.3 V LSMtronsupercap module
	10 Nos of 10 F, 3 V SC
switches	PMOS - IXTH20P50P, NMOS - IRFB7434 and IRFP4905
	PVN102 PV relay
LED lamps	12 V, 5.5 W PHILIPS LED lamps
micro-controller	PIC16F684
MOSFET driver	IRS4427
opto-isolator	4N25
timer IC	LM555
regulators	LM338, LM7805
transformer	1:1 toroidal transformer (custom design)

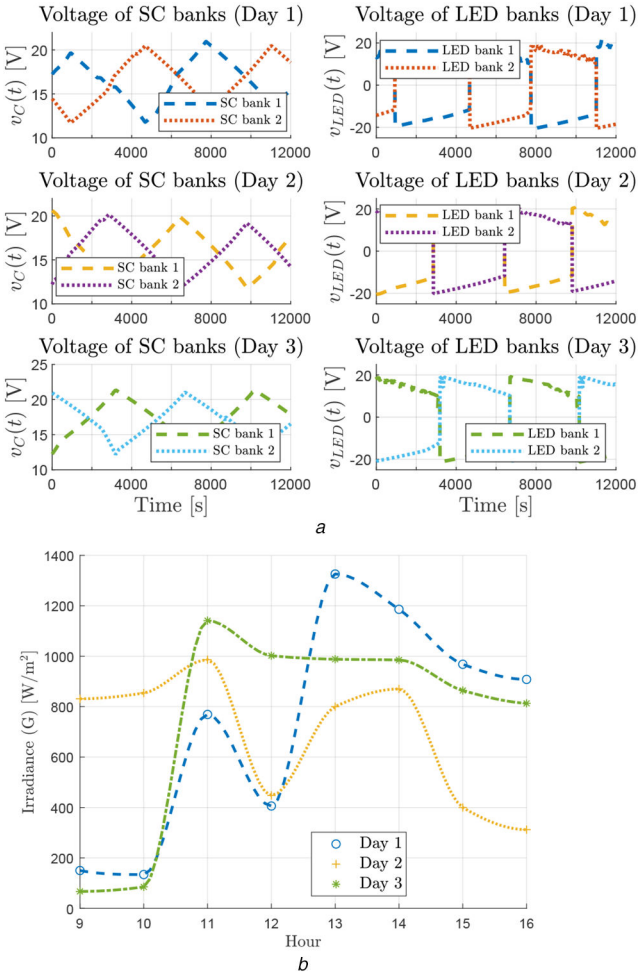

Fig. 25 *Operational behaviour of SCALED converter installed in POAL DCMG container*

(a) Experimental results of SCALED converter, ***(b)*** Variation of irradiance throughout the day in POAL site

levels of 730, 643 and 744 Wm^{-2} is shown in Fig. 25. Fig. 25*a* shows the voltage across two SC banks and two LED banks. 20 W LED lamp loads were used on both sides of the converter. Irradiance variations throughout the day (from 0900 to 1600 h) was recorded using an irradiance meter and depicted in Fig. 25*b*.

The ETEE of overall system was calculated using (18) and experimental results are shown in Table 9. When considering the ETEE of the power stage, power consumption of the control circuits was disregarded, since controller consumption is constant irrespective of the size of the LED lamp loads and the SC bank size. By observing the experimental results and comparing them with simulation results in Fig. 23, SCALED technique has

Table 9 Summary of experimental results of SCALED converter

Parameter	Specification
operating voltage range of SC banks (LED bank)	20 – 12 V
switching losses	250 mW
ETEE	88.9–94%
switching frequency	0.15×10^{-3} Hz
switching period	$\simeq$ 2 hours
autonomy time (depends on the lamp load)	15 to 30 min

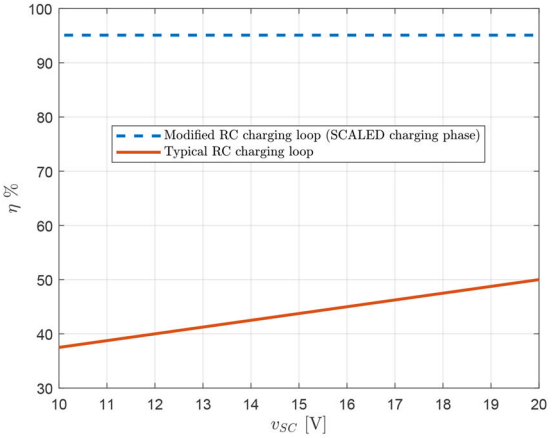

Fig. 26 *Comparison of charging efficiency between direct SC bank replacing battery pack and SCALED converter*

achieved the target of ETEE over 85%. Using this proposed system, it is possible to achieve higher ETEE levels in the range of 88.9% to 94%.

$$\eta = \frac{P_{\text{out}}}{P_{\text{in}}} = \frac{\overline{V_{\text{LED1}}} \cdot \overline{i_{\text{LED1}}} + \overline{V_{\text{LED2}}} \cdot \overline{i_{\text{LED2}}}}{\overline{V_{\text{solar}}} \cdot \overline{i_{\text{solar}}}} \tag{18}$$

where over-bar denotes average over time.

It is important to highlight here that the above range of efficiencies were achieved without using any MPPT type DC–DC converter, since impedance matching required in MPPT is not practicable in this case, due to SC banks used for temporary energy storage. By examine Fig. 25, it is obvious that this configuration is capable of buffering against irradiance fluctuations. This is due to the fact that LED lamps can be operated across a wide range of positive and negative voltages without degrading the brightness with the SC banks acting as energy buffers to smooth out irradiance fluctuations. In addition this technique provides short-term DC-UPS capability in case of a sudden power loss. During testing, authors established that the switching frequency of the converter was well below 1 Hz for small loads. This frequency increases with the size of the LED lamp load. Results obtained from this testing are summarised in Table 9.

Fig. 26 compares the two possibilities for demonstrating the efficiency advantage of the SCALED converter. If a battery pack is replaced by a pre-charged SC bank, for efficiency we end up in the case of lower graph in Fig. 26, whereas by inserting an LED lamp load into the loop while charging the SC bank it is possible achieve a significant efficiency gain, as demonstrated in Fig. 15 and upper graph in Fig. 26. This is due to the fact that SC banks are charged with a series LED lamp load (acting as the useful R_{L} in Fig. 14*b*), utilising the 'wasted' energy in the *RC* charging loop.

In summary, the main features and advantages of this novel converter are

- Higher ETEE with SC banks acting as lossless droppers
- No high frequency DC–DC converters required thus eliminating RFI/EMI issues

• Short term DC-UPS capability for irradiance fluctuations, by over-sizing the SC banks, thus eliminating the need for battery banks

Compared to the high frequency switching converters coupled with a complex processor algorithm to achieve MPPT in a battery based system achieving an ETEE around 90% [34], SCALED technique is able to achieve efficiencies in the range of 88.9–94%, while maintaining the switching frequency in an extra-low range such as few Hz to fractional Hz.

7 Conclusion

By combining unique properties of LED lamps with SC banks, a novel loss circumventing SCALED converter for DC lighting in buildings is developed. This SC-based technique achieves significantly high ETEE, has short-term DC-UPS capability, and has the ability to cater for fluctuations in renewable energy source. A secondary advantage is the ability to overcome RFI/EMI issues due to its very low frequency switching associated with a large time constant *RC* circuit formed by a SC bank and the LED luminaries.

8 Acknowledgments

Authors of this paper gratefully acknowledge the opportunities created by POAL to test and install the SCALED system in their DCMG container, with special thanks to the team led by sustainability manager of POAL Rosie Mercer.

9 References

[1] Kularatna, N.: 'Supercapacitor assisted low dropout regulators (SCALDO) for high efficiency DC-DC converters for DC microgrid applications'. 2015 IEEE First Int. Conf. on DC Microgrids (ICDCM), Atlanta, USA, 2015, pp. 333–338

[2] Singh, R.: 'Report of DC Energy Efficiency Committee'. IEEE Power and Energy Society, Washington, DC, 29 July 2014

[3] Vossos, V., Garbesi, K., Shen, H.: 'Energy savings from direct-DC in U.S. residential buildings', *Energy Build.*, 2014, **68**, pp. 223–231

[4] Backhaus, S., Swift, G.W., Chatzivasileiadis, S.*, et al.*: '*DC microgrids scoping study: estimate of technical and economic benefits*' (Los Alamos National Laboratory, New Mexico, 2015)

[5] Ayai, N., Hisada, T., ShibaTa, T.*, et al.*: '*DC micro grid system*' (SEI Technical Review, Tokyo, Japan, 2012)

[6] Elsayed, A.T., Mohamed, A.A., Mohammeda, O.A.: 'DC microgrids and distribution systems: an overview', *Electr. Power Syst. Res.*, 2014, **2**, pp. 407–417

[7] Singh, R., Alapatt, G.F., Bedi, G.: 'Why and how photovoltics will provide cheapest electricity in the 21st century', *Electron. Energ.*, 2014, **27**, (2), pp. 275–298

[8] Jayananda, D., Kularatna, N., Steyn Ross, D.A.: 'A validity of MPPT technique using supercapacitors as energy storage devices: example of the SCALED converter technique'. 45th Annual Conf. of the IEEE Industrial Electronics Society 2019 (IECON), Lisbon, Portugal, 2019, pp. 515–520

[9] Rezk, H., Eltamaly, A.M.: 'A comprehensive comparison of different MPPT techniques for photovoltaic systems', *Sol. Energy*, 2015, **112**, pp. 1–11

[10] Dolara, A., Faranda, R., Leva, S.: 'Energy comparison of seven MPPT techniques for PV systems', *J. Electromagn. Anal.Appl.*, 2009, **3**, pp. 152–162

[11] Babaa, S.E., Armstrong, M., Pickert, V.: 'Overview of maximum power point tracking control methods for PV systems', *Power Energy Eng.*, 2014, **2**, pp. 59–72

[12] de Brito, M.A.G., Sampaio, L.P., Junior, L.G.*, et al.*: 'Evaluation of MPPT techniques for photovoltaic applications'. 2011 IEEE Int. Symp. on Industrial Electronics., Gdansk, Poland, 2011, pp. 1039–1044

[13] de Brito, M.A.G., Sampaio, L.P., Luigi, G.*, et al.*: 'Comparative analysis of MPPT techniques for PV applications'. 2011 Int. Conf. on Clean Electrical Power (ICCEP), Ischia, Italy, 2011, pp. 99–104

[14] Adly, M., Ibrahim, M., El Sherif, H.: 'Comparative study of improved energy generation maximization techniques for photovoltaic systems'. 2012 Asia-Pacific Power and Energy Engineering Conf., Shanghai, China, 2012, pp. 1–5

[15] Subudhi, B., Pradhan, R.: 'A comparative study on maximum power point tracking techniques for photovoltaic power systems', *IEEE Trans. Sustain. Energy*, 2013, **4**, (1), pp. 89–98

[16] Gunawardane, K., Kularatna, N.: 'Supercapacitor-assisted low dropout regulator technique: a new design approach to achieve high-efficiency linear DC-DC converters', *IET Power Electron.*, 2017, **1**, pp. 1–10

[17] SAMWHA Capacitor Co. L., Capacitors, S., (Eds.): 'ESD-SCAP Catalogue, SAMWHA Capacitor Co., Ltd., 2018'. (SAMWHA Capacitor Co. Ltd, 2018

[18] Green, M.A., Emery, K., Hishikawa, Y.*, et al.*: 'Solar cell efficiency tables (version 45)', *Prog. Photovolt., Res. Appl.*, 2015, **23**, pp. 1–9

[19] Eltawil, M.A., Zhao, Z.: 'MPPT techniques for photovoltaic applications', *Renew. Sustain. Energy Rev.*, 2013, **25**, pp. 798–813

[20] Brito, M.A.G.D., Galotto, L., Sampaio, L.P.*, et al.*: 'Evaluation of the main MPPT techniques for photovoltaic applications', *IEEE Trans. Ind. Electron.*, 2013, **60**, (3), pp. 1156–1167

[21] Panizza, M.: '*Input source impedance and its effects on DC-DC converter performance and characteristics*' (Vicor Corporation, Andover, USA, 2009)

[22] Kularatna, N.: 'Supercapacitors improve the performance of linear power-management circuits: unique new design options when capacitance jump from micro-farads to farads with a low equivalent series resistance', *IEEE Power Electron. Mag.*, 2016, **3**, (1), pp. 45–59

[23] Kankanamge, K., Kularatna, N.: 'Improving the end-to-end efficiency of DC-DC converters based on a supercapacitor-assisted low-dropout regulator technique', *IEEE Trans. Ind. Electron.*, 2014, **61**, (1), pp. 223–230

[24] Gurusinghe, N., Kularatna, N., Round, W.H.*, et al.*: 'Energy-limited transient-mode fast supercapacitor charger topology', *IEEE Trans. Power Electron.*, 2017, **32**, (2), pp. 911–914

[25] Fernando, J., Kularatna, N., Round, H.*, et al.*: 'Implementation of the supercapacitor-assisted surge absorber (SCASA) technique in a practical surge protector'. 40th Annual Conf. of the IEEE Industrial Electronics Society (IECON 2014), Dallas, USA, 2014, pp. 5191–5195

[26] Ariyaratna, T., Jayananda, D., Kularatna, N.*, et al.*: 'Potential of supercapacitors in novel power converters as semi-ideal lossless voltage droppers'. 43rd Annual Conf. of the IEEE Industrial Electronics Society (IECON 2017), 2017, pp. 1429–1434

[27] Kularatna, N., Fernando, J.: 'Inventors; Hamilton (NZ) WaikatoLink Limited, assignee: High current voltage regulator'. US 9707430B2, Hamilton, New Zealand, 2011

[28] Kankanmage, K., Kulatana, N.: 'Supercapacitor assisted LDO (SCALDO) techniquean extra low frequency design approach to high efficiency DC–DC converters and how it compares with the classical switched capacitor converters'. 2013 28th Annual IEEE Applied Power Electronics Conf. and Exposition (APEC), Long Beach, USA, 2013, pp. 1979–1984

[29] Kularatna, N.: '*DC power supplies power management and surge protection for power electronic systems*' (CRC Press, Tylor and Francis Group, 6000 Broken Sound Parkway NW, Suite 300, Boca Raton, USA, 2012)

[30] Matulka, R., Wood, D., Department, E.*, et al.*: '*The history of the light bulb online at: energy.gov/articles/history-light-bulb*' (Department of Energy Facilities, Washington DC, USA, 2013)

[31] Jayananda, D., Kularatna, N., Steyn Ross, D.A.: 'Powering 12-V LED luminiaries with supercapacitor-based energy storage in DC-microgrid systems'. 44th Annual Conf. of the IEEE Industrial Electronics Society (IECON 2018), Washington DC, USA, 2018, pp. 1922–1927

[32] Jayananda, D., Kularatna, N., Steyn Ross, D.A.: 'Design Approach for Supercapacitor Assisted LED lighting (SCALED) technique for DC-microgrids'. 2018 IEEE International Conference on Industrial Electronics for Sustainable Energy Systems (IESES), Hamilton, New Zealand, 2018, pp. 27–31

[33] Jayananda, D., Kularatna, N., Steyn Ross, D.A.: 'Supercapacitor assisted LED lighting (SCALED) for DC-micro grids'. 2019 IEEE Third Int. Conf. on DC Microgrids (ICDCM), Matsue, Japan, 2019, p. to be published

[34] Chowdhury, S.A., Mourshed, M.: 'Off-grid electrification with solar home systems: an appraisal of the quality of components', *Renew. Energy*, 2016, **97**, pp. 585–598